Turbulent sediment transport processes in energetic sediment-laden open-channel flows varying from clear water, non-capacity to full transport capacity conditions

Hélder Guta, David Hurther, Julien Chauchat

Turbulent sediment transport processes in energetic sediment-laden open-channel flows varying from clear water, non-capacity to full transport capacity conditions

H. Guta,
D. Hurther
J. Chauchat
Laboratory of Geophysical and Industrial Flows (LEGI), Univ. Grenoble Alpes, CNRS, Grenoble-INP, France

ABSTRACT: A new dataset of co-located 2C velocity, sediment concentration and sediment flux profile measurements collected with an Acoustic Concentration and Velocity Profiler (ACVP), are presented in this paper. The experimental protocol developed herein is described in details. The first results are displayed in terms of mean velocity, concentration and sediment flux profiles. The validity of the logarithmic velocity profile and the Rouse concentration profile for the suspension load are analyzed. The effect of the Shields and suspension numbers on the solid transport mode is discussed. The flow quantities and turbulent transport processes to be analyzed with this new High-Resolution dataset and the corresponding questions to be addressed are raised in the conclusion.

1 INTRODUCTION

Reliable and accurate predictions of sediment transport rate, as a product of velocity and concentration profiles over the entire flow, remains an important scientific challenge, particularly during energetic flow forcing such as floods which control the long-term morphological evolution of rivers. Concerning the velocity prediction, there is still debate on the universality of the value of the von Karman constant κ. Coleman 1981 and Cellino & Graf 1999 argued that the universal value ($\kappa = 0.41$) provides good results, if the wake coefficient due to free-surface flow effects is properly evaluated. However, its reduction in sediment-laden flows has been reported in early studies (Vanoni 1946) and more recently based on experimental (Revil-Baudard at al. 2015, 2016) and numerical evidence (Cheng et al. 2018, Advances in Water Resources). Another challenge concerns the concentration profile prediction. Although the Rouse profile is a physically based model, it is often required to tune the parameter in the exponent that describes the ratio between the momentum and particle diffusivities, called the Schmidt number (Cellino 1998, Cellino & Graf 1999).

With the aim of addressing these questions, this study consisted in producing a new dataset of sediment transport experiments using light-weight solid particles measured with the ACVP technology (Hurther et al. 2011) in energetic open-channel flows generated in the LEGI tilting flume. Three hydrodynamic forcing conditions are defined, in terms of bed slope and water discharge. For each condition, four sediment-laden flow conditions are examined, varying from clear water, 2 non-capacity and the full transport capacity (saturation) conditions. For each condition, the corresponding hydraulic and sediment transport regime is characterized in terms of dimensionless Reynolds, Roughness, Froude, Shields and suspension numbers.

In order to improve our understanding of the physical processes involved in sediment transport, and thus improve our capability to model this energetic particle transport mode, the need of high resolution measurements resolving small turbulent flow scales is evident. The ability to profile

within particle-laden high-Reynolds number shear-boundary layer flows remains currently limited to a few measurement technologies, such as gamma-ray and conductivity techniques in pipe flows, capacitance probes, boroscopic probes, video technique for instantaneous 2C particle velocity and mean concentration profiles. In the recently past years, an Acoustic Concentration and Velocity Profiler (Hurther et al. 2011, Fromant et al. 2018, 2019) has been developed, and revealed new insights into hydrodynamic and sediment transport processes in the near-wall region. This technology has been applied here to measure collocated and instantaneous 2C velocity and concentration profiles and the results are well described in (Revil-Baudard et al 2015,2016). However, important limitations of these studies were linked to the experimental protocol inducing short duration (120 s) of the experimental runs. These limitations imposed a repetition of many repeatable runs in order to perform an ensemble average for sufficient statistical convergence of the measured turbulent flow quantities. As a consequence of this time-demanding experimental protocol the range of studied hydraulic and sediment transport parameters was very narrow. Additionally, it did not allow analysis of long-term evolution of sediment transport for which continuous measurements of turbulent quantities over several minutes are necessary.

In the present study, the new sediment-feeding unit is tested and evaluated for reaching a wide range of aimed hydraulic and sediment transport regimes. A new protocol is proposed and validated allowing long experimental runs under well-controlled conditions.

2 METHODOLOGY

2.1 *Experimental setup and flow properties*

The experiments were carried out at the LEGI, using a 10 m long tilting flume, with 0.35 m width. The particles used in the present experiments are low density (ρv=1192 kg/m3) irregularly shaped plastic particles (Poly-Methyl MethAcrylate) of median diameter d_p = 3 mm. The settling velocity of the particles is $w_s = 5.6$ cm/s (Revil-Baudard et al. 2015). The fixed bed is covered by glued particles, with the same properties as the sediments transported by the flow. The flow was highly turbulent, hydraulically rough and subcritical (Table 1), as indicated by the high Reynolds number ($Re = 4UR_h/\nu > 2000$), the high bed roughness Reynolds number ($Re* = u\,k_s/\nu > 70$) and the low Froude number ($Fr = U/\sqrt{gH_f}$<1).

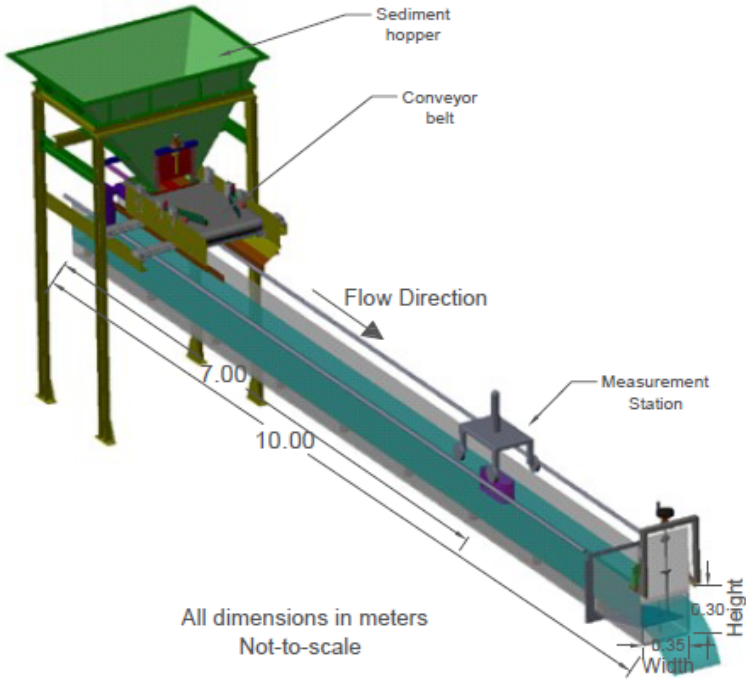

Figure 1. Sketch of experimental set up

The use of a Honey comb at the flume inlet and the rough channel bed over the 6m upstream the measurement section located...m downstream the inlet, guarranties the full development of the turbulent shear boundary layer (Revil-Baudard 2014). The sediment injection point is located ...m upstream the measurement setion for reaching fully developed sediment transport conditions in the flow transverse and vertical directions. One paragraph with comments on distance of the injection point to the measurement point, Honey comb and rough surface at the entry to enhance boundary layer development etc etc.

Table 1. Flow conditions and hydraulic parameters, for PMMA with d_{50} = 3 mm

u_* (m/s)	θ (-)	S (-)	Q (m^3/s)	S_0 (-)	U (m/s)	H_f (m)	Re (-)	Fr (-)	Re* (-)	q_s (m^2/s)	C	Runs
0.043	0.33	1.3	0.032	0.0023	0.60	0.15	$1.9x10^5$	0.49	323	0.0	0.0	8 runs
										$6x10^{-5}$	$5x10^{-4}$	P3S03D4_LOW,P3S03D5_LOW,P3S03D6_LOW
										$2x10^{-4}$	$2x10^{-3}$	P3S03D4_MED,P3S03D7_MED,P3S03D8_MED
										$3x10^{-4}$	$3x10^{-3}$	P3S03D9_SAT,P3S03D10_SAT,P3S03D11_SAT
0.056	0.56	1.0	0.041	0.0040	0.79	0.15	$2.5x10^5$	0.65	421	0.0	0.0	8 runs
										$7x10^{-5}$	$6x10^{-4}$	P3S05D1_LOW,P3S05D2_LOW,P3S05D8_LOW
										$2x10^{-4}$	$2x10^{-3}$	P3S05D1_MED,P3S05D2_MED,P3S05D8_MED
										$6x10^{-4}$	$5x10^{-3}$	P3S05D3_SAT,P3S05D4_SAT,P3S05D5_SAT
0.068	0.81	0.8	0.049	0.0061	0.96	0.15	$3.0x10^5$	0.80	509	0.0	0.0	8 runs
										$9x10^{-5}$	$6x10^{-4}$	P3S08D3_LOW,P3S08D7_LOW,P3S08D9_LOW
										$3x10^{-4}$	$2x10^{-3}$	P3S08D2_MED,P3S08D8_MED,P3S08D9_MED
										$9x10^{-4}$	$7x10^{-3}$	P3S08D2_SAT,P3S08D3_SAT,P3S08D5_SAT

S_0: Slope of the channel; U: bulk mean velocity; H_f: water depth; ν: kinematic viscosity of water; u_*: friction velocity; ks: equivalent roughness (ks=2.5 dp for mobile bed experiments and ks=3 mm for clear water) and g is the gravitational acceleration

The experiments are performed in sequence of at least two runs, consisting of one clear-water flow for reference, followed by 1 - 3 sediment-laden flow runs, each with a duration of 300 s. Thus, the maximum number of experimental runs in the same sequence was limited to four. No modifications in the experimental set up was performed from clear-water to the subsequent sediment-laden flow runs. This ensured that they were all performed in the exact same configuration, with only the addiction of sediments as the vector of change in the hydrodynamic conditions. Furthermore, one can define the position of rigid fixed bed for all sediment-laden runs based on the CW runs. Once the CW run was completed, the feeding unit was turned on, beginning the injection of the sediments. Before start recording the sediment-laden run, a delay was necessary for the flow to be established in presence of particles. This time varied in different hydraulic and transport regimes, ranging between 60 – 90 s. It was estimated by analyzing the time necessary for reaching a constant time-rate of sediment transport .

For each forcing condition, three set of measurements in which each one included one clear-water and three solid transport regimes were carried out. The number of experimental runs can be estimated as: $Nb\ runs\ =\ 3\ flow\ regimes\ x\ 4\ transport\ regimes\ x\ 3\ experiments\ =\ 36\ runs$. In general, most sequence of measurements included one CW run and only one or two solid transport regimes. This resulted in a high number of clear-water runs obtained to cover all desired transport regimes. Thus, eight CW runs were obtained for each hydraulic condition.

The injected solid load in full-capacity was defined experimentally, as function of the progressive saturation of the sediment trnasport rate associated with beginning of sediment deposition at the bed. The two other transport regimes were fixed as function of the mean concentration $C = qs_{injected}/Q$. The defined mean volumetric concentrations are approximately $6x10^{-5}$ and $2x10^{-4}$, for the lower and the intermediate transport regimes, respectively. The same values of mean concentration for under capacity regimes were defined for all forcing conditions. This will allow to compare sediment-laden flows with the same mean concentration in different turbulence

conditions. The defined values are in the range in which of dilute suspension, as referred in the literature (Cellino & Graf 1999).

2.2 *Experimental protocol*

A sediment feeder is used to continually inject a pre-determined solid load into the flow. The solid load injection can be accurately controlled by the speed of the conveyor belt and the positions of the outlet vane of the sediment container. The speed of the conveyor belt is set by the electric tension of its motor. Thus, a calibration was necessary in terms of tension – speed – solid load. After determining a relationship of conveyor belt tension – speed, a relationship tension – $qs_{injected}$ was obtained independently. The injected solid load was defined as the (packed) volume of sediment collected in a recipient divided by the corresponding time interval of filling. Since the graduated recipient has a maximum capacity of 12 liters, it limited the duration of the tests to 40 – 240 s, depending on the feeding velocity. The referred durations are lower than the experimental runs, but the stability and constancy in the functioning of feeding unit allows it to be representative of the mean solid load over much longer durations. Regarding the uncertainties in estimating $qs_{injected}$, the potential error in the measurement of the deposited volume and the corresponding time were estimated as 0.5 l (constant for all measurements) and 1 s (increasing 2% for each decimal unit of voltage). The resulting estimated uncertainties for the injected solid load remained below 10%. As the properties of the particles are similar to previous studies (Revil-Baudard et al. 2015, Fromant et al. 2018), the same porosity of the packed bed (p = 45%) is used. This imply a packed-bed volumetric concentration of 0.55. Figure 2 displays the obtained relationship tension – injected solid load for a given set of controlling parameters. It is observed that the solid discharge varies linearly with the velocity, thus, one can set the tension according to the desired solid load. The obtained calibration curve is valid for a given set of geometrical parameters: opening of vertical gate h_t=10.0 mm, position of horizontal plate h_h=78.8 mm using wet sediments.

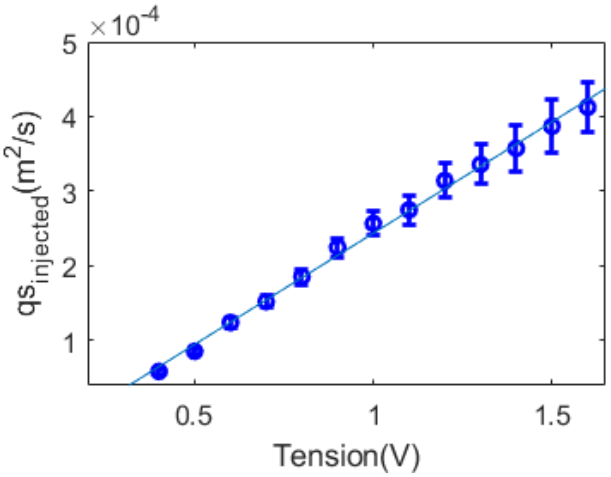

Figure 2. Calibration of solid load as function of tension of the conveyor belt. The uncertainties in each measured are represented independently, which a minimum of 5% (for Tension = 0.4) and a maximum of 9% (for Tension = 1.5).

2.3 *ACVP technology and measurements validation*

The velocity profiling principle relies on the measurement of Doppler frequencies using pulse-to-pulse coherent demodulation. By employing one emitter (that emits sound pulses at a given frequency) and two receivers, two bistatic Doppler frequencies along the common emitter axis can be measured. The streamwise velocity *u* and the flow normal velocity *w* are then obtained from the Doppler Shift frequencies.

The concentration profiling is determined from the inversion of the echo intensity signal. The output of the mean squared voltage signal of the ACVP is (Hurther et al. 2011):

$$I = A_j A_s C exp\left(-4 \int_0^r \zeta_s C \, dr\right) \quad (1)$$

The term A_j includes the system dependent parameters and the water absorption term along the profile. The term A_s is the particle scattering term. The ζ_s is the attenuation coefficient and C is the particle mass concentration. A vertical resolution (1.5 mm) allows the discretization of Equation 2 in order to estimate vertical profile of C explicitly (Hurther et al. 2011). The mean sediment flux is estimated over the time interval of the experimental run (t = 300 s):

$$q_s = K * \frac{1}{T} \int_{t1}^{t1} \int_{zb}^{Hf} u(z,t)\phi(z,t) dz dt \quad (2)$$

A constant K is calibrated to fit the injected solid load, determined as explained in subsection 2.1. This calibration is performed for the intermediate hydraulic and solid transport regimes (P3S05D1_MED, P3S05D2_MED and P3S05D8_MED), and then it is verified for the two other hydraulic and transport regimes. Figure 3 displays the comparison between the solid load measured from ACVP and the injected solid. The figure includes more experimental runs than those displayed in Table 1. This was necessary to test the ACVP performance over a wider range of transport conditions.

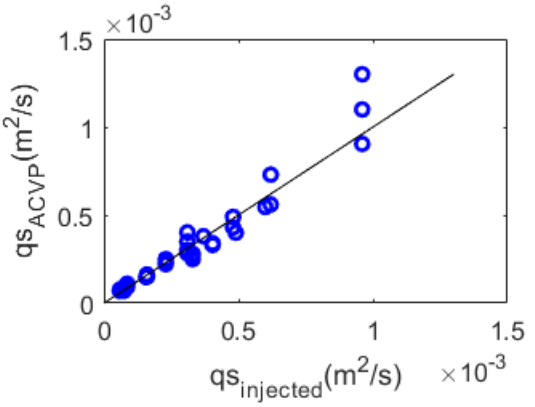

Figure 3. Comparison $qs_{ACVP\ vs}$ $qs_{injected}$ Solid line is X=Y.

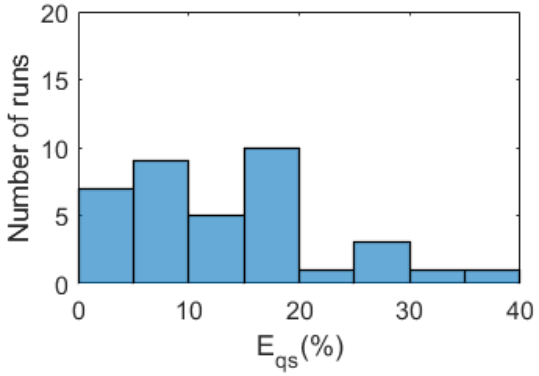

Figure 4. Histogram of E% of qs_{ACVP}

In Figure 3, the alignment of the points with the solid line which represents the 100% correlation suggests a good agreement of the ACVP measurements with the predetermined solid load. This is observed over a wide range of transport regimes. The accuracy of the measurements are quantified by the relative error, estimated as $E(\%) = (|qs_{ACVP}| - qs_{injected})/qs_{injected}$. In Figure 4, the histogram of the relative error is displayed. In general, the relative error in the mean solid load measured by ACVP remained below 30% overall. Few exceptions were observed in the range of 30 - 40 %. This result supports the capability of the ACVP technology to measurement sediment transport in such challenging flow conditions, as shown in previous studies (Revil-Baudard et al. 2015, 2016, Fromant et al. 2018).

2.4 *Repeatability of the experimental protocol*

In this subsection, the similarity in the trend of experiments performed in the same hydraulic and solid transport regimes is presented. Figure 5 displays the time evolution of the accumulated volume of transported sediments over the entire duration of the run, for all the solid transport runs.

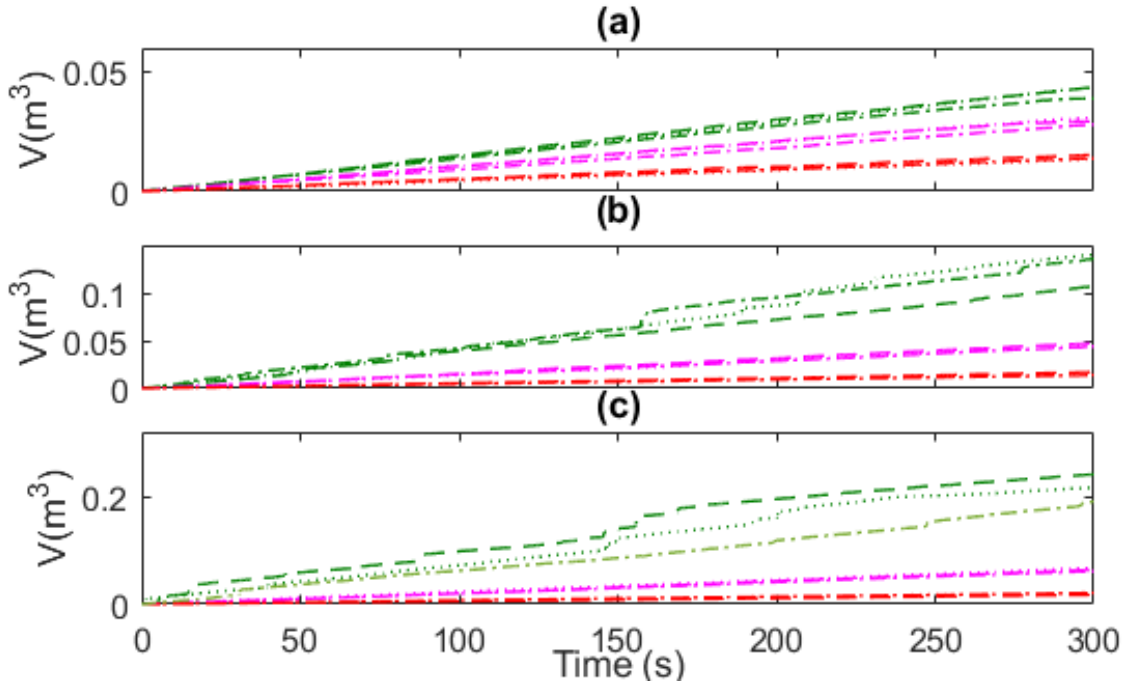

Figure 5. Accumulated volume of transported sediments, for Fr = 0.49 a), Fr = 0.65 b) and Fr = 0.8 c). In each plot, the set of curves with lower (in red), intermediate (magenta) and higher (green) slopes corresponds to lower, intermediate and higher solid transport regime, respectively.

A set of 3 runs for each transport regime is displayed. One observes that they display similar trends. In some cases, they are almost superimposed, suggesting that they were identical. Differences are observed in the saturated (full-capacity) regime, mainly due to the sudden variations of the solid transport caused by the incipient deposition, as referred previously.

The linear trend of the measured transported sediment volume confirms that the runs of sediment-laden flows were recorded after the transport is well established. The bumps observed for the cases of in-capacity regimes are associated with the incipient deposition of particles in the bed. An intermittent saturation is observed in the near-bed region, results in periods of relatively high solid transport.

3 RESULTS

In this section, preliminary results in terms of mean flow quantities are displayed for velocity, concentration and sediment flux profiles. In Figure 6 are presented the mean profiles, for the intermediate hydraulic regime ($Fr = 0.65$) of three experimental runs. As described in Table 1, P3S05D8_LOW, P3S05D8_MED and P3S05D8_SAT, correspond to lower , intermediate and saturated (full capacity) transport regimes.

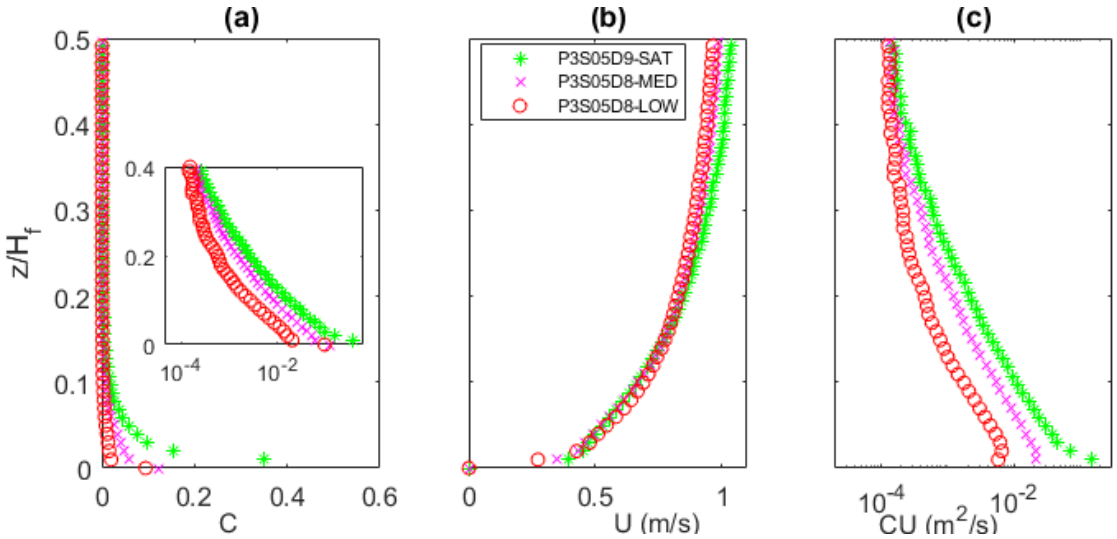

Figure 6. Mean profiles of concentration a) velocity b) and sediment flux c).

The mean velocity in Figure 6b reveal the well-known logarithmic shaped profile with distance from the bed, particularly in the lower layer ($z/H_f < 0.20$) named the inner flow region (Nezu and Nakagawa 1993). The velocity profiles of the different runs are similar supporting the same hydraulic regimes for the three conditions, despite small differences noticed in the outer flow region. The mean concentration and sediment flux profiles illustrate the difference in terms of transport rate. With a Shields number $\theta = \rho_f u_*^2 / (\rho_p - \rho_f) g d_p = 0.56$ and a suspension number $S = w_{s/u_*} = 1.0$, the regime corresponds to sheet-flow for which there is an equilibrium between suspension and bed-load transport following the classification proposed by Sumer et al. (1996).

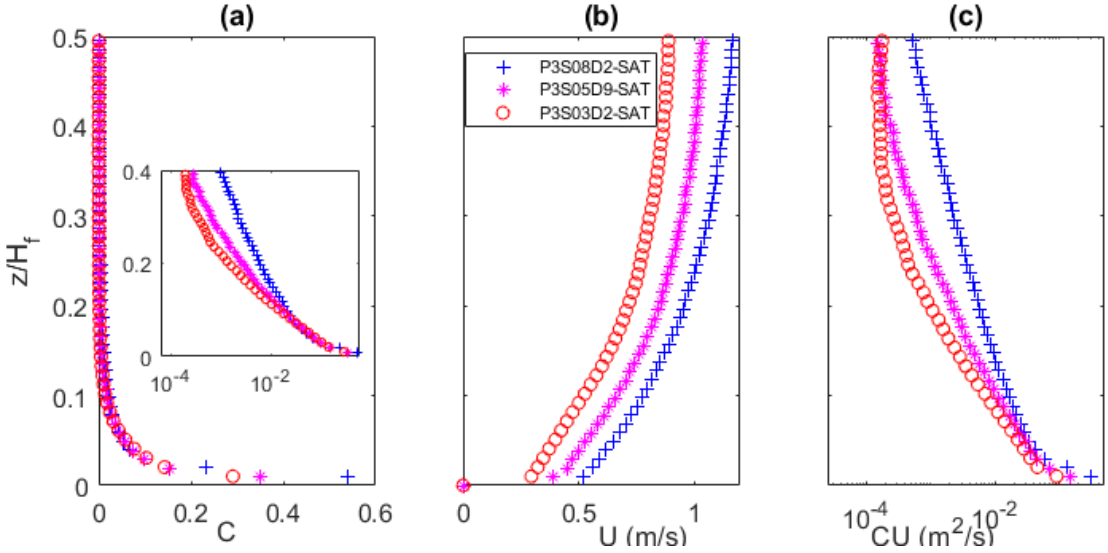

Figure 7. Mean profiles of concentration a) velocity b) and sediment flux c).

The transport is mostly in suspension when the injected solid load are far below capacity, as observed from the lower than 8% values of the mean concentration over the entire profile for the low transport regime (mean volumetric concentration $C = 7 \times 10^{-5}$). As the injection rate is increased to the intermediate case ($C = 2 \times 10^{-4}$), the concentration values exceed the critical suspension value of 8% and the solid transport profiles show a clear increase particularly for $0 < z/H_f < 0.35$. With further increase up to capacity regime, the concentration profile displays the typical shape of a Rouse profile in the upper suspension layer where the mean concentration is lower than

8%. In the near-bed region $0 < z/H_f < 0.04$, the profile deviates from the Rouse profile with high concentration values and gradients typical of a bedload sublayer.

In Figure 7, mean profiles of concentration, velocity and sediment flux are displayed for three different hydraulic conditions at full transport capacity conditions. The Shields number and the suspension number vary for each case, thus, the transport mode is modified accordingly. As described in Table 1, the hydraulic conditions are clearly distinct in the three cases. Figure 7b shows the increase of the magnitude of the mean velocity profile, from the less energetic (P3S03D2-SAT) to the most energetic sediment-laden flows (P3S08D2-SAT). Since they are all in capacity conditions, the concentration profiles (Figure 7a) exhibit a Rouse shape. However, differences in the extension of the concentration and sediment flux profiles over the flow depth indicates the different modes of transport.

As presented in Table 1, the less energetic flow has a Shields number $\theta = 0.35$ and suspension number $S = 1.2$. This suggests that it is essentially bed-load transport, with low proportion of suspension. This can be observed in the concentration and sediment flux profile, as they decrease from relatively high values in the near-bed region to near zero more rapidly than the other regimes. The intermediate case was discussed previously and displayed in Figure 6. The most energetic case has a Shields number $\theta = 0.85$ and suspension number $S = 0.80$. This suggests that the proportion as suspended-load is similar or greater than the fraction transported as a bedload. The measurements support this prediction as one observes in Figure 7a and 7c that run P3S08D2-SAT displays broader profiles. Indeed, it can be seen that the vertical position in which the sediment flux reaches nearly zero is approximately $z/H_f = 0.30$ and $z/H_f = 0.40$ for lower and intermediate regime whereas it corresponds to approximately $z/H_f = 0.6$ for the most energetic regime.

4 DISCUSSION AND CONCLUSIONS

An new experimental protocol of sediment transport measurements has been developed. The repeatability of the protocol allowed producing a new dataset of sediment flux processes, covering a wide range of dimensionless numbers. In the present study, preliminary results in terms of mean velocity, concentration and sediment flux were presented. The typical trend described by the law of the wall has been observed in the velocity profiles. The concentration profiles display the typical Rouse shaped profiles for the suspended load and the presence of bedload layers in certain cases.

With the dataset presented herein, the following quantities will be studied: Reynolds shear and normal stresses, turbulent velocity spectra, turbulent mixing length, turbulent eddy and sediment diffusivities, TKE production, dissipation and transport terms. This should help addressing several open questions:

- How does the von Karman constant and the Schmidt number value evolve over a large range of shields and suspensions number.
- Can we confirm the existence of two modes of transport in terms of Schmidt number? What are the underlying sediment transport mechanisms?
- What is the contribution of turbulent (horizontal and vertical) sediment flows to total transport? How do these relative contributions evolve over a wide range of numbers Shields and suspension numbers?
- What role play coherent flow structures known as ejection and sweeps in the suspension and bedload layers and how is the dynamics of the bed affected?

REFERENCES

Cellino, M. (1998). An experimental study of suspension flow in open-channels. PhD thesis n°1824, *Ecole Polytechnique Fédérale de Lausanne*, Switzerland.

Cellino, M. and Graf, W. H. (1999). Suspended sediment-laden Flow in Open Channels under non-Capacity and Capacity Condition. Aw. Soc. Civ. Eng., J. Hydr. Engn, vol. 125,N".5, pp. 455-462.

Cheng, Z., Hsu, T.-J. and Chauchat, J. (2018). An eulerian two- phase model for steady sheet flow using large-eddy sim- ulation methodology, Advances in Water Resources 111, 205.

Fromant, G., R. S. Mieras, T. Revil-Baudard, J. A. Puleo, D. Hurther, and J. Chauchat. 2018. "On Bedload and Suspended Load Measurement Performances in Sheet Flows Using Acoustic and Conductivity Profilers." *J. Geophys. Res. Earth Surf.* 123(10):2546–62. doi: 10.1029/2017JF004560.

Fromant, Guillaume, David Hurther, Joep Van der Zanden, D. A. Van Der A, I. Caceres, Tom O'Donoghue, and J. S. Ribberink. 2019. "Wave Boundary Layer Hydrodynamics and Sheet Flow Properties under Large-scale Plunging-type Breaking Waves." *J. Geophys. Res. Ocean.* 124(1):75–98.

Hurther, D., Thorne, P. D., Bricault, M., Lemmin, U. & Barnoud, J.M. (2011) A multifrequency acoustic concentration and velocity profiler (ACVP) for boundary layer measurements of fine-scale flow and sediment transport processes. Coastal Engineering. 58, 594–605.

Nezu, I., and H. Nakagawa. 1993. *Turbulence in Open Channel Flows*. A. A. Balkema, Rotterdam.

Revil-Baudard, T., Chauchat, J., Hurther, D. & Barraud, P. A. (2015) Investigation of sheetflow processes based on novel acoustic high-resolution velocity and concentration measurements. J. Fluid Mech. 767, 1–30.

Revil-Baudard, T., Chauchat, J., Hurther, D. & Eiff, O. A. (2016) Turbulence modifications induced by the bed mobility in intense sediment-laden flows. J. Fluid Mech., 808, 469 - 484.

Sumer, B. M., Kozakiewicz, A., Fredsøe, J. & Deigaard, R. (1996) Velocity and concentration profiles in sheet-flow layer of movable bed. ASCE J. Hydraul. Eng 122 (10), 549–558.

Vanoni, V. A. E. J. 1946 Transportation of suspended sediment by running water. Trans. Am. Soc. Civ. Eng. 111, 67–133